Quantum signatures of chaos in a cavity-QED-based stimulated Raman adiabatic passage

Amit Dey*
Ramananda College, Bankura University, Bankura 722122, India
and International Centre for Theoretical Sciences, Tata Institute of Fundamental Research, Bengaluru 560089, India

(Received 20 November 2020; revised 23 March 2021; accepted 19 April 2021; published 11 May 2021)

Nonlinear stimulated Raman adiabatic passage (STIRAP) is a fascinating physical process that dynamically explores chaotic and nonchaotic phases. In a recent paper [A. Dey and M. Kulkarni, Phys. Rev. Res. **2**, 042004(R) (2020)], such a phenomenon is realized in a cavity-QED platform. There, the emergence of chaos and its impact on STIRAP efficiency are mainly demonstrated in the semiclassical limit. In the present paper we treat the problem in a fully quantum many-body framework. With the aim of extracting quantum signatures of a classically chaotic system, it is shown that an out-of-time-ordered correlator (OTOC) measure precisely captures chaotic and nonchaotic features of the system. The prediction by OTOC is in precise matching with classical chaos quantified by Lyapunov exponent analysis. Furthermore, it is shown that the quantum route corresponding to the semiclassical followed state encounters a dip in single-particle purity within the chaotic phase, depicting a consequence of chaos. A dynamics through the chaotic phase is associated with spreading of the many-body quantum state and an irreversible increase in the number of participating adiabatic eigenstates.

DOI: 10.1103/PhysRevA.103.053704

I. INTRODUCTION

A cavity-QED (c-QED) system is an interesting platform that holds immense potential of implementing quantum networks [1–6], quantum information processing and communication [1,7–9], efficient quantum simulators for many-body systems [10–13], etc. The light-matter interaction in a cavity-QED offers Jaynes-Cummings (JC)-like [14–16] and Bose-Hubbard-like [17] nonlinearities at various regimes of parameters. Such nonlinear features result in exciting novel phenomena such as photon self-trapping [14,15,18], nonlinear transport [19,20], and chaos [16,21–23].

Chaos, in classical systems, is well defined as the sensitivity to the initial condition and the exponential divergence of trajectories (with slightly different initial conditions) with time. However, the nature of manifestation, mechanisms, and diagnostics of chaos in the quantum counterpart of classically chaotic systems is relatively less established and is an active area of research. Equilibration of closed quantum systems is a fundamentally important open question and it can be a consequence of chaos in their classical counterparts [24,25]. Quantum chaos also delves into the deep connections among localization of quantum-mechanical wave functions, quantum-classical transitions, and decoherence mechanisms [26], and deals with irreversibility in quantum systems with few degrees of freedom [27]. Therefore, understanding such features in complex quantum systems and their correspondence with classical counterparts demands a thorough theoretical and experimental investigation. A number of platforms have explored the quantum characteristics of classically chaotic systems. Some of them are optical realizations of kicked harmonic oscillators [28], ultracold atoms [29–31], atom-optics realization [32], and cavity-QED setups [23,33,34].

While the sensitivity to initial conditions for classical systems is quantified by Lyapunov exponent (LE) analysis, the corresponding quantum systems usually reflect integrability via level spacing statistics of eigenvalue spectra [35,36], participation number of eigenstates [22,37], the out-of-time-ordered correlator (OTOC) [38,39], etc. OTOC measures the dispersion of information (initially localized with a few degrees of freedom) to an exponentially large number of degrees of freedom, thereby resulting in an apparent loss of local quantum information and distribution of correlation throughout the entire system [40–42]. This so-called scrambling of quantum information is considered to be an efficient diagnostic of many-body quantum chaos [33,34,43–47]. Furthermore, OTOC is shown to be a very reliable measure of quantum chaos compared to traditional level spacing statistics measurement [48]. The practical measurement of OTOC is quite challenging due to the need of back evolution during measurement [43] and has been achieved in a limited number of systems [45–47]. Therefore, seeking efficient strategies [43] and physical systems with high-precision controllability is imperative.

Stimulated Raman adiabatic passage (STIRAP) is a process of remarkable utility and has been exploited in fields such as atomic population transfer, optical applications, state preparation and state transfer for quantum information processing, and many more [49,50]. The presence of "dark states" connecting only terminal nodes of a network facilitates a robust adiabatic transfer which is immune to dissipation originating from intermediate nodes [49,50]. STIRAP for many-particle systems with interparticle interactions can be treated efficiently in the classical mean-field approximated framework. The dynamics of field amplitudes (describing node populations) is described by the nonlinear Schrödinger

*amit.dey.85@gmail.com

equation, where the nonlinear term is produced by interparticle interaction [51]. In the present context the light-matter interaction, which was shown to generate photon-photon interaction [14,17], leads to the study of nonlinear STIRAP [16]. In the absence of light-matter interaction the studied case becomes the standard linear STIRAP. In a fully quantum-mechanical treatment the probability amplitudes evolve according to the linear Schrödinger equation. However, it is interesting to see the traces of mean-field nonlinearity on the quantum-mechanical evolution of STIRAP.

Nonlinear interaction in an adiabatic passage induces qualitative changes in its mean-field stationary energy levels and results in breakdown of adiabaticity [51–53]. Nonlinear STIRAP explores phases of varying integrability during a single sweep and is an excellent process to investigate chaos [16,37,54,55]. The transition from nonchaotic (or regular) to chaotic phase simply by controlling tunable system parameters makes nonlinear STIRAP immensely interesting. Cavity-QED-based STIRAP is usually studied in the context of state preparation with a three-level atom coupled to cavity mode [49,56,57]. In contrast our cavity-QED STIRAP models three spatially separate cavities with one of them containing a qubit. We are looking for an adiabatic process that leads to photon population transfer between terminal cavities without populating the central cavity. The photon-qubit interaction provides the scope for studying the impact of nonlinearity on the transfer process [16]. We proposed an efficient photon transfer protocol in a precisely controllable and scalable cavity-QED network in Ref. [16], where chaos emerges during a STIRAP due to JC-like nonlinearity. In the present paper, we extend the analysis beyond the semiclassical treatment in Ref. [16] and handle the problem in a quantum many-body framework. We show that the quantum process (corresponding to the semiclassical STIRAP) undergoes a spreading of its evolved many-body state within the chaotic parameter window, predicted by semiclassical theory. This is associated with irreversible increase in the participation number of adiabatic eigenstates of the system. A qualitative comparison is made between LE analysis (for the semiclassical case) and microcanonical OTOC measurement (for the quantum many-body case). It shows a remarkable agreement in (semiclassically predicted) chaotic and nonchaotic regimes of the process. Additionally, the semiclassical followed state (which is nearly a dark state) is shown to be constituted of a series of diabatic transitions through the avoided crossings between many-body eigenstates. The many-body state corresponding to this followed state produces a dip in single-particle purity within the chaotic window.

The paper is arranged as follows. In Sec. II the model Hamiltonian is introduced and equations for stationary point (SP) solutions are deduced. Section III deals with the quantum eigenspectrum and its features in the chaotic regime. LE analysis and OTOC measurement are elaborated in Sec. IV and single-particle purity calculation for the quantum states (corresponding to the semiclassical followed state) is presented in Sec. V. The chaotic effects on the slow-sweep real-time dynamics along with behavior of participation number are described in Sec. VI. Section VII deals with the sweep rate dependence of transfer efficiency and its behavior with varying photon number. Sections VIII and IX present the level spacing statistics and open-system dynamics, respectively. Finally, we conclude and discuss potential future directions of our analysis in Sec. X.

II. MODEL, EQUATIONS OF MOTION, AND SCHEME

We studied cavity-QED STIRAP in a semiclassical framework in Ref. [16]. We observed emergence of chaotic stages due to light-matter interactions and worked out strategies for obtaining efficient photon transfer between terminal cavities of a cavity-QED network. As already mentioned in the introduction, by the chaotic stage we mean the STIRAP stage [characterized by J_1, J_2 values in Eq. (1)] where two trajectories with slightly different initial conditions diverge exponentially, thereby producing very different final states. This means that while evolving through the chaotic stages any small deviation can dislodge the system from the desired followed state (that leads to successful adiabatic passage) and results in inefficient transfer.

In this section our starting point is the same Hamiltonian as dealt with in Ref. [16] but in contrast to our earlier work we analyze the Hamiltonian with purely quantum considerations. The cavity-QED STIRAP Hamiltonian is given by

$$\hat{H}(\tilde{t}) = \sum_{j\in\{a,b,c\}} \hat{H}_j - J_1(\tilde{t})(\hat{a}^\dagger\hat{b} + \text{H.c.}) - J_2(\tilde{t})(\hat{b}^\dagger\hat{c} + \text{H.c.}), \tag{1}$$

where the JC Hamiltonian for cavity a is defined as $\hat{H}_a = \omega_a\hat{a}^\dagger\hat{a} + \Omega_a\hat{s}_a^z + g_a(\hat{a}^\dagger\hat{s}_a^- + \text{H.c.})$. $\hat{a}$ and g_a are the photon destruction operator and JC coupling intensity for cavity a, respectively. The qubit is described by the spin operator s_a^α ($\alpha \in \{x, y, z\}$). Ω_a and ω_a denote the frequencies for qubit and photon modes, respectively. The time-varying coupling parameters are $J_{1,2}(\tilde{t}) = K\exp[-(\tilde{t} - \tilde{t}_{1,2})^2]$ (where the relation $\tilde{t}_1 > \tilde{t}_2$ fixes the sequence of pump and Stokes pulses) with the parametric time defined as $\tilde{t} \equiv t/\tau$ [16]. This in turn parametrizes the time-dependent Hamiltonian $\hat{H}(t)$, making it only implicitly dependent on time t. The sweep rate of couplings is given by $\dot{\tilde{t}} = 1/\tau$ and is a key factor for STIRAP dynamics [16]. Throughout the paper we use the values $\tilde{t}_1 = 3.697, \tilde{t}_2 = 2.4242$ and consider the resonant case $\omega_{a,b,c} = \Omega_{a,b,c}$ for all the numerical results. To draw correspondence with the semiclassical results of Ref. [16] we also consider a setup, where $g_a = g_b = 0$, $g_c \neq 0$ and $\omega_{a,c} = \omega_b - \Delta$ (where Δ is central cavity detuning and is fixed at $\Delta = 0.5K$ throughout the paper, if not specified separately). Such a nonuniformity for $g_{a,b,c}$ has two aspects. First, the Fock state $|n_a, n_b, n_c, s_c^z\rangle \equiv |N, 0, 0, -1/2\rangle$ becomes the eigenstate at $\tilde{t} = 0$; this is advantageous for initialization keeping experimental realization in mind. Here, n_j, s_j^z are the eigenvalues of the operators $\hat{n}_j$, $\hat{s}_j^z$, respectively. Second, $g_b \neq 0$ does not alter our findings regarding efficient adiabatic passage, because cavity b remains negligibly occupied throughout the process. However, incorporating these assumptions and projecting $\hat{H}$ in the rotating frame of ω_a the new Hamiltonian can be rewritten as

$$\hat{H}(\tilde{t}) = \Delta\hat{n}_b + g_c(\hat{c}^\dagger\hat{s}_c^- + \text{H.c.}) - J_1(\tilde{t})(\hat{a}^\dagger\hat{b} + \text{H.c.}) - J_2(\tilde{t})(\hat{b}^\dagger\hat{c} + \text{H.c.}). \tag{2}$$

The semiclassical approximation $\langle \hat{a}^\dagger \hat{s}_a^- \rangle \approx \langle \hat{a}^\dagger \rangle \langle \hat{s}_a^- \rangle$ is valid in the large N limit [14,16]. We employ the Heisenberg equation of motion with respect to $\hat{\mathcal{H}}(\tilde{t}) = \hat{H}(\tilde{t}) - \mu(\tilde{t})(\hat{n}_a + \hat{n}_b + \hat{n}_c + \hat{s}_c^z + 1/2)$ and apply the above approximation. Furthermore, replacing the expectation values as $\{\langle \hat{a} \rangle, \langle \hat{b} \rangle, \langle \hat{c} \rangle, \langle \hat{s}_c^- \rangle, \langle \hat{s}_c^z \rangle\} \to \{a, b, c, s_c, s_c^z\}$ and setting the time derivatives to zero, we obtain the equations for SP solutions given by

$$J_1 b + \mu a = 0, \tag{3}$$

$$\Delta b - J_1 a - J_2 c - \mu b = 0, \tag{4}$$

$$J_2 b - g_c s_c + \mu c = 0, \tag{5}$$

$$2 g_c \, c \, s_c^z + \mu s_c = 0. \tag{6}$$

Here μ is the chemical potential accounting for the conservation $\sum_{j\in\{a,b,c\}} n_j + [s_c^z + 1/2] = N$ [16]. The energies $E_{\rm SP}$ corresponding to the SP solutions of Eqs. (3)–(6) are plotted as black dots in Figs. 1 and 2.

The quantum dynamics of the system is dictated by Schrödinger's equation

$$i\dot{\psi}(t) = \hat{H}\psi(t), \tag{7}$$

where $\psi(t)$ is the quantum-mechanical wave function, which is prepared as the Fock state $|\psi(0)\rangle = |N, 0, 0, -1/2\rangle$ at $t = 0$ ($\tilde{t} = 0$). For linear STIRAP (when $g_{a,b,c} = 0$) the system state is prepared as $|\psi(0)\rangle = |N, 0, 0\rangle$ and the complete adiabatic sweep (from $\tilde{t} = 0$ to $\tilde{t}_f$) translates the system to the desired state $|\psi(\tilde{t}_f)\rangle = |0, 0, N\rangle$. This scheme is implemented by following the two-cavity coherent eigenstate [37] given by

$$|\psi_d\rangle_{\tilde{t}} = \frac{1}{\sqrt{N!}}[\cos\Theta(\tilde{t})\hat{a}^\dagger - \sin\Theta(\tilde{t})\hat{c}^\dagger]^N |\text{vac}\rangle, \tag{8}$$

where $\cos\Theta = J_2/\sqrt{J_1^2 + J_2^2}$. $|\psi_d\rangle_{\tilde{t}}$ does not project on cavity b and is equivalent to the semiclassical dark state. The nonlinear version of $|\psi_d\rangle_{\tilde{t}}$ slightly deviates from Eq. (8) for moderate values of g_c. In the next section we elaborate the semiclassical adiabaticity when viewed from a quantum many-body perspective.

III. EIGENSPECTRUM AND SP SOLUTIONS

Here we plot the eigenvalue spectrum for various g_c values and investigate its characteristics in the classically chaotic and nonchaotic regimes. The eigenenergies E_ν (with eigenstate index ν) of the quantum Hamiltonian [Eq. (2)] are obtained by diagonalizing $\hat{H}(\tilde{t})$ at various $\tilde{t}$'s and plotted by solid continuous lines in Figs. 1 and 2. In Fig. 1(a) the $g_c = 0.1K$ case is presented. There are $(N+1)^2$ (which is the size of the Hilbert space) number of eigenvalues $E_\nu(\tilde{t})$ in contrast to only a few semiclassical $E_{\rm SP}$'s. The particular $E_{\rm SP}$ branch, that we follow to achieve cavity-a to cavity-c transfer by negligibly populating cavity b, is designated by a series of black arrows beside it. This *nearly dark* state (note, the dark state is exactly defined for linear STIRAP $g_{a,b,c} = 0$ [16,49]) is the special SP (SSP) branch of our interest. In Fig. 1(b) it is clearly seen that the SSP branch ($E_{\rm SSP}$) passes through a series of avoided crossings between many-body eigenstates. Therefore,

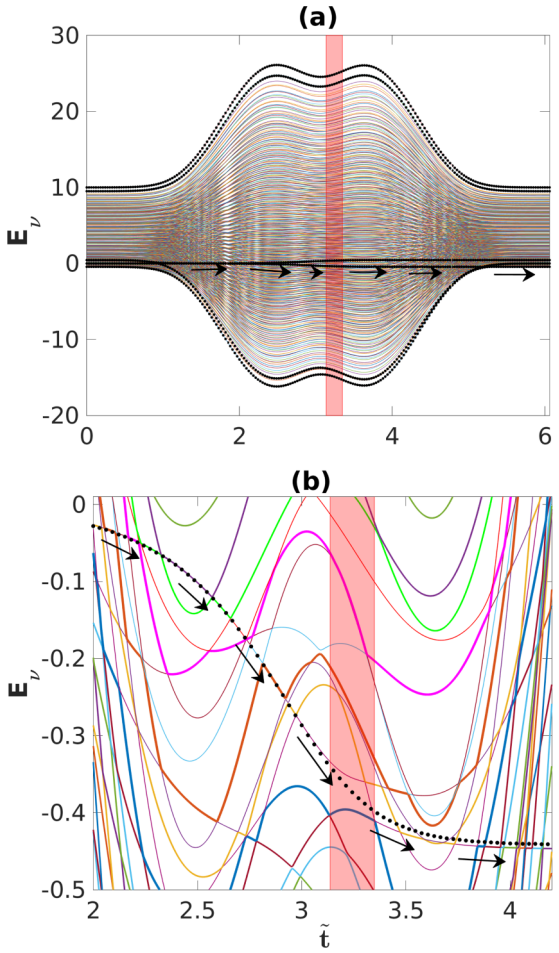

FIG. 1. For $g_c = 0.1K$ quantum many-body eigenenergies with varying $\tilde{t}$ are plotted as colored solid lines. The semiclassically obtained $E_{\rm SP}$ solutions are plotted by black dots and the red vertical patch marks the semiclassically obtained chaotic window of $\tilde{t}$, predicted by LE analysis in Sec. IV. (a) Full spectrum of many-body eigenenergies. (b) Zoomed version of panel (a) showing that the followed SSP branch corresponds to a series of avoided crossings of quantum-mechanical eigenlevels. In grayscale different energy levels participating in avoided crossings (along SSP) are distinguished by varying thickness and shades of solid lines. The black arrows in panels (a) and (b) direct the SSP branch $E_{\rm SSP}$ that leads to near-unity photon transfer from cavity a to cavity c with negligible occupancy of cavity b.

the adiabatic following of classical SSP is actually numerous diabatic transitions among eigenstates (at an avoided crossing location) in the many-body scenario. Interestingly, unlike the avoided crossings in the nonchaotic region, the avoided crossings within the chaotic window of $\tilde{t}$ lack proximity between participating eigenstates. This actually portrays an enhancement of level repulsion within the chaotic window and disrupts the quantum diabatic route corresponding to the classical SSP branch. At the exit of the chaotic window the quantum route via *closely* avoided crossings is again formed along the SSP branch. Therefore, classically predicted chaos is remarkably manifested by enhanced level repulsion of the quantum eigenspectrum, whereas the $E_{\rm SSP}$ solution gives no trace of chaos. It should be noted that the chaotic window

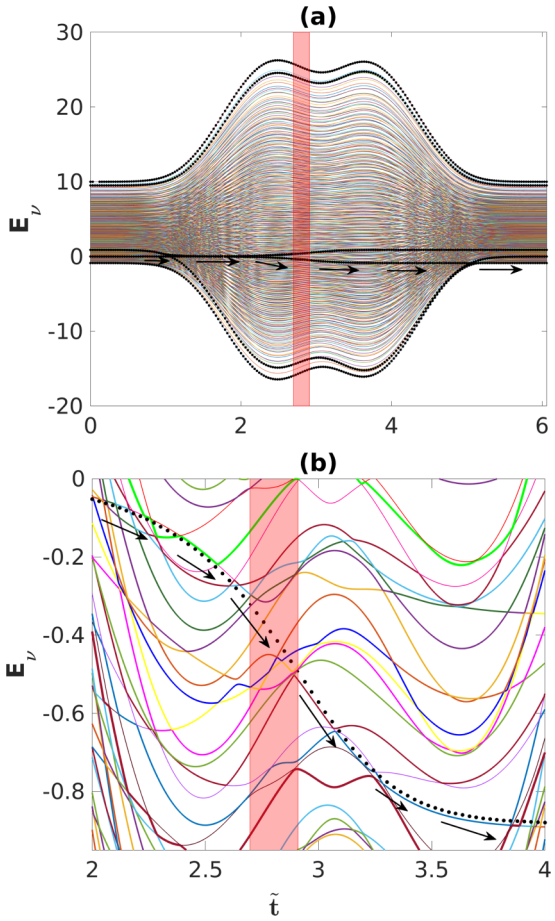

FIG. 2. For $g_c = 0.2K$ quantum many-body eigenenergies with varying $\tilde{t}$ are plotted as colored solid lines. The semiclassically obtained $E_{\rm SP}$ solutions are plotted by black dots and the red vertical patch marks the semiclassically obtained chaotic window of $\tilde{t}$, predicted by LE analysis in Sec. IV. (a) Full spectrum of eigenenergies. (b) Zoomed version of panel (a) showing that the followed SSP branch corresponds to a series of avoided crossings of quantum-mechanical eigenlevels. In grayscale different energy levels participating in avoided crossings (along SSP) are distinguished by varying thickness and shades of solid lines. The black arrows in panels (a) and (b) direct the SSP branch $E_{\rm SSP}$ that leads to near-unity photon transfer from cavity a to cavity c with negligible occupancy of cavity b.

[red patch in Figs. 1(a) and 1(b)] is drawn by LE analysis presented in Sec. IV. To strengthen our observation we present $g_c = 0.2K$ in Fig. 2 and observe similar features of eigenspectra as in Fig. 1. Here too within the classically chaotic region the eigenvalues do not facilitate diabatic transitions by enhancing level repulsion.

At this point it is important to recall the standard energy-level crossing prescription [37] motivated by linear Landau-Zener transition [58–61]. For a pair of energy levels ν, ν' engaged in an avoided crossing, the diabatic transition between the levels requires $1/\tau \gg d^2_{\nu,\nu'}/\sigma_{\nu,\nu'}$, where $d_{\nu,\nu'} = (E_\nu - E_{\nu'})$ and $\sigma_{\nu,\nu'} = |\langle\nu|\partial_{\tilde{t}}\,\hat{H}(\tilde{t})|\nu'\rangle|$ at the avoided crossing location. This depicts the dependence of dynamics on the rate of change of the Hamiltonian. In other words, when eigenvalues in a pair are widely apart and have a smaller gradient at their closest proximity (which is the case for participating eigenlevels within the chaotic window), diabatic transition becomes challenging, requiring a very fast sweep of $J_{1,2}$.

In the next section we quantify chaos for both semiclassical and quantum cases and draw a comparison.

IV. LYAPUNOV ANALYSIS AND OTOC MEASURE

For a classically chaotic system the phase-space trajectories are extremely sensitive to the initial conditions. Two trajectories, which are infinitesimally separated in the phase space at $t = 0$, exponentially diverge with time, resulting in a completely varied outcome at long times. Chaos is quantified by the LE providing the rapidity of divergence. We consider a reference trajectory to be characterized by SSP solution at a particular $\tilde{t}$ and a test trajectory initially δ_0 separated (with respect to the reference trajectory) in the phase space. Both the trajectories are evolved for a time step ξ followed by a reset of the test trajectory such that the new phase-space distance δ_1 between the trajectories becomes δ_0 along the same direction as δ_1 [62–66]. The procedure is repeated for a large number of steps M and the LE is extracted as

$$\lambda_M = \lim_{\delta_0 \to 0} \frac{1}{MK\xi} \sum_{j=1}^{M} \log\left(\frac{\delta_j}{\delta_0}\right). \tag{9}$$

Here, δ_j denotes the phase-space distance just before the jth reset. The maximum LE $\lambda_{\rm max}$ is defined for $M \to \infty$, whereas the finite-time LE λ_M measures the divergence for an evolution time $t = KM\xi$. This procedure is advantageous compared to the usual procedure because the phase space for our system is bounded due to the constraint $n_a + n_b + n_c + s^z_c + 1/2 = N$ and this does not allow a monotonic growth of distance between the trajectories.

Now for a quantum counterpart of the classically chaotic system chaos is captured by the exponential growth of the commutator of observables, provided that the initial commutator value is considerably small [33,34,39–47]. The thermal OTOC is defined as

$$O(t)_T = -\langle [U(t), V(0)]^2 \rangle_T, \tag{10}$$

where U and V are two operators; $\langle ... \rangle_T$ denotes the thermal average defined as $\langle \hat{A} \rangle_T = Z^{-1} \sum_n \langle n|\hat{A}|n\rangle e^{-\beta\epsilon_n}$ where $\beta = 1/k_B T$, ϵ_n is the energy of the energy eigenstate $|n\rangle$, and Z is the partition function. In our analysis we only focus on the particular energy eigenstates corresponding to the followed SSP branch and deal with the microcanonical OTOC defined as $O_\nu(t) = \langle\nu|[\hat{n}_a(t), \hat{n}_c(0)]^2|\nu\rangle$ [23,39]. At $t = 0$ $\hat{n}_a$ and $\hat{n}_c$ commute. Expanding $O_\nu(t)$ in the energy eigenbasis we write it as

$$O_\nu(t) = \sum_{\nu'} |\langle\nu|[\hat{n}_a(t), \hat{n}_c(0)]|\nu'\rangle|^2. \tag{11}$$

In Fig. 3(a) we plot the LE (corresponding to $E_{\rm SSP}$) at three representative $\tilde{t}$ values and obtain a positive LE for $\tilde{t} = 2.7879$ falling within the chaotic window marked in Fig. 2. In contrast, $\lambda_{\rm max} \to 0$ for $\tilde{t}$ on either side of the window, indicating nonchaotic regions [16]. Figure 3(b) plots the microcanonical OTOC for eigenstates having energies closest to $E_{\rm SSP}$. We observe an exponential increase in O_ν [inset of Fig. 3(b)]

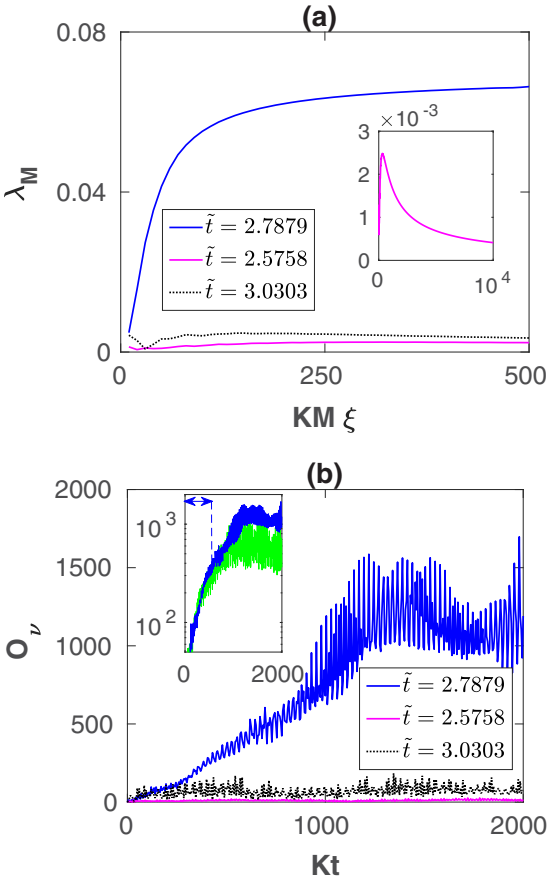

FIG. 3. Depicting quantum-classical comparison of chaos for $g_c = 0.2K$. (a) LE plots at three representative $\tilde{t}$ values: $\tilde{t} = 2.7879$ [solid blue (black)] within the chaotic window introduced in Fig. 2 and $\tilde{t} = 2.5758$ [solid magenta (gray)] and 3.0303 (dotted black) at either side of the window. (b) OTOC plots at the same $\tilde{t}$ values for eigenstates [of the fixed Hamiltonian $H(\tilde{t})$] along semiclassical $E_{\rm SSP}[\tilde{t}]$. Here, the selective eigenstates are $|\nu\rangle \equiv |169\rangle, |164\rangle, |158\rangle$ for $\tilde{t} = 2.5758, 2.7879, 3.0303$, respectively. The inset in panel (a) shows that the LE is asymptotically approaching zero for non-chaotic $\tilde{t}$. The inset in (b) plots log-scaled O_ν for the $\tilde{t} = 2.7879$ case and an additional instance for $\tilde{t} = 2.7273$ [green (gray) for $|\nu\rangle = |165\rangle$] within the chaotic window. The vertical blue dashed line marks exponential growth of O_ν followed by a saturation region.

only for $\tilde{t}$ that produces a positive $\lambda_{\rm max}$ in its semiclassical counterpart. The exponential growth of O_ν tends to saturate at long times.

V. ONE-PARTICLE PURITY

The one-particle density matrix is very useful for extracting information about many-body quantum systems [67,68]. Expectation values of single-particle operators are resourceful measurable quantities for experiments. A one-particle reduced density matrix is obtained by integrating out degrees of freedom of $N-1$ particles from the N-particle density matrix [67]. The purity of the one-particle density matrix quantifies coherence of one-particle states of a whole system [37,69].

In this section we analyze the single-particle purity along the quantum-mechanical diabatic route for cavity-a to cavity-c transfer of photons. The single-particle purity is defined as

$$\gamma = \text{Trace}([\rho^{sp}]^2). \tag{12}$$

Here the single-particle reduced density matrix corresponding to the N-particle eigenstate $|\nu\rangle$ is defined as

$$\rho^{sp}_{i,j} = (1/N)\langle\nu|\hat{A}^\dagger_i \hat{A}_j|\nu\rangle, \tag{13}$$

where $\hat{A}_i \equiv \{\hat{a}, \hat{b}, \hat{c}, \hat{s}^-_c\}$ and $|\nu\rangle$ is the eigenstate of interest. Note that the flipping of the qubit from ground to excited state is associated with absorption of one photon and $\hat{s}^+_c \hat{s}^-_c$ is quantitatively equivalent to one photon excitation. γ falls within the range $\{1/4, 1\}$. When $\gamma = 1$ the many-body eigenstate is a coherent state having localized distribution in the phase space. On the other hand, $\gamma = 1/4$ corresponds to a maximally mixed state. In Fig. 4 we plot γ along the quantum diabatic route corresponding to the classical adiabatic SSP branch. We pick $|\nu\rangle$ along the classically adiabatic route $E_{\rm SSP}$ and calculate γ. We observe that γ has a sharp dip in the regime where the system is classically chaotic. Moreover, for stronger g_c the depth of the dip increases. This is because the phase-space distribution of the adiabatic eigenstate spreads over the chaotic zone and considerably deviates from being a coherent state [37]. Therefore, the strong reduction of single-particle purity is reflected here as a consequence of chaos.

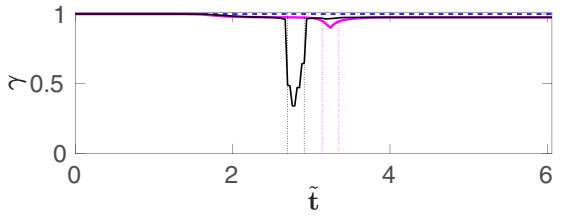

FIG. 4. One-particle purity at various $\tilde{t}$ for eigenstates along the SSP solutions. $g_c = 0, 0.1K, 0.2K$ are plotted as dashed blue, solid magenta (gray), and solid black, respectively. The corresponding chaotic windows are marked by vertical dotted lines of the same color.

So far we have dealt with features of the eigenspectrum at various $\tilde{t}$'s falling inside and outside the chaotic window. In the subsequent sections we explore their consequences on the real-time dynamics of the system and on the STIRAP efficiency.

VI. QUANTUM DYNAMICS AND CHAOTIC SPREADING

Here we investigate the chaotic effects on the real-time dynamics of the system. It is to be noted that the dynamics very much depends on the sweep rate $1/\tau$ [16] (i.e., how fast the system Hamiltonian is tuned), although the eigenspectrum only depends on the parametric time $\tilde{t}$ [i.e., on $\hat{H}(\tilde{t})$ in Eq. (2)]. The slower-sweep semiclassical dynamics initiated at the SSP branch at $t = 0$ starts oscillating about the SSP branch within the chaotic window, thereby diminishing the transfer efficiency [16]. For a quantum case we initiate the system in the Fock state $|\psi(0)\rangle \equiv |N, 0, 0, -1/2\rangle$ and the dynamics is studied using the Schrödinger equation given by Eq. (7). Within the chaotic window the evolved many-body state $|\psi(t)\rangle$ suffers a spreading over the adiabatic eigenstates supported by the chaotic energy range.

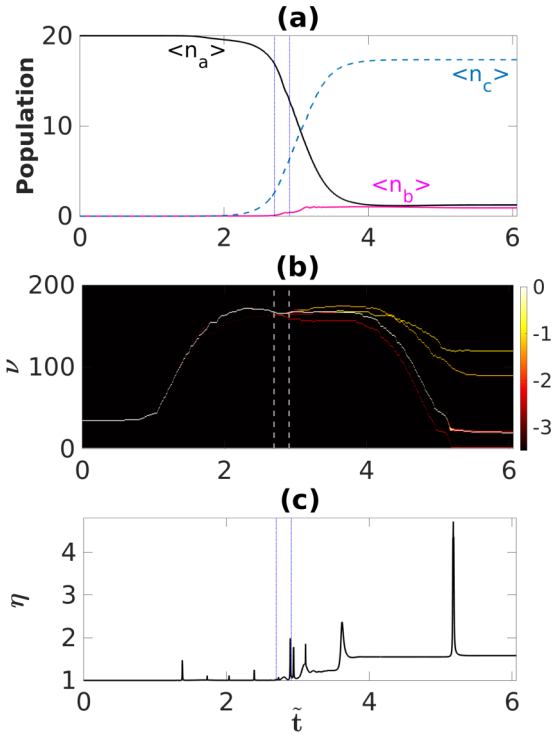

FIG. 5. (a) Real-time quantum dynamics of cavity populations for $g_c = 0.2K$, when the system is initialized to $|n_a, n_b, n_c, s_c^z\rangle \equiv |20, 0, 0, -1/2\rangle$ at $\tilde{t} = 0$ and swept at a rate $1/\tau = 0.003K$. (b) Probability distribution over adiabatic eigenstates for the dynamics described in panel (a). The color coding for probability distribution is logarithmically scaled. (c) Dynamics of participation number corresponding to panel (a). Vertical dotted lines in all three panels mark the chaotic window.

Figure 5 describes the dynamics through various $\tilde{t}$ values for the specified sweep rate $1/\tau$. In Fig. 5(b) we plot the probability distribution over the adiabatic eigenstates while the slow-sweep dynamics is carried out. It is clear that the system's many-body state spreads out exactly within the semiclassically predicted chaotic window and the consequence is reflected in the diminished transfer (from cavity a to cavity c) in Fig. 5(a). Moreover, the cavity-b population starts increasing within the chaotic window deteriorating the STIRAP protocol. The spreading can be quantified by the participation number of eigenstates in the evolved state $|\psi(t)\rangle$ and is given by

$$\eta(t) = 1 \Big/ \sum_{\nu} |\langle \nu | \psi(t) \rangle|^4, \tag{14}$$

where $1/\eta$ is termed as the inverse participation ratio. In Fig. 5(c) η shows only reversible spikes ($1 < \eta < 2$) before reaching the chaotic window. These occur due to the diabatic transitions while evolving. In contrast, the increment of η within the chaotic window irreversibly goes beyond 2 and distinctively portrays a nonchaotic-to-chaotic transition. Therefore, the signature of chaos in a quantum framework is expressed as spreading of the evolved state and irreversible growth of participation number [22,37].

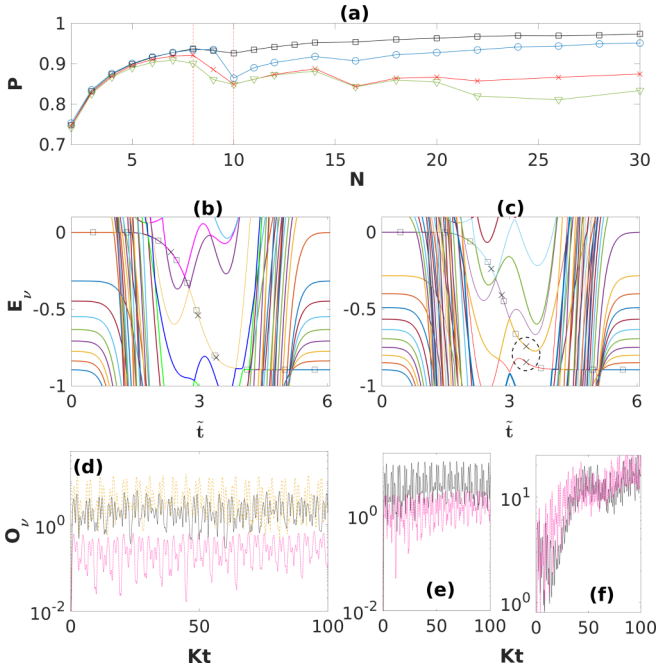

FIG. 6. (a) Efficiency P plotted with varying total excitation number N and for $g_c\sqrt{N} = 0.8944K$, $\Delta N = 10K$, $J_{1,2}N = 20K\exp[-(\tilde{t} - \tilde{t}_{1,2})^2]$. Cases with sweep rates $1/\tau = 0.0606K, 0.0152K, 0.003K, 0.0015K$ are plotted by square, circle, "×," and triangle line types, respectively. Vertical dashed lines mark $N = 8$ and 10. The eigenvalue spectra are plotted for (b) $N = 8$ and (c) 10, respectively. Squares in panels (b) and (c) describe the route (composed of a series of avoided crossings) that leads to cavity-a to cavity-c photon transfer. The dashed circle in (c) indicates the region where the energy gap between participating eigenstates becomes much wider, disrupting the diabatic crossing. (d–f) O_ν is plotted in logarithmic scale for eigenstates on the followed route at various $\tilde{t}$ and these states are marked by "×" in panels (b) and (c). O_ν plots in panel (d) corresponding to panel (b) are for $\{\tilde{t}, \nu\}$: $\{2.3333, 33\}$ [dotted magenta (gray)], $\{2.9697, 31\}$ (dashed orange), and $\{3.3939, 31\}$ (solid black). Panel (e) corresponds to panel (c) for $\{2.5758, 48\}$ [dotted magenta (gray)] and $\{2.8182, 46\}$ (solid black). Panel (f) corresponds to panel (c) for $\{3.3939, 44\}$ [dotted magenta (gray)] and $\{3.3939, 45\}$ (solid black).

In the next section we explore transfer efficiency with varying sweep rate and investigate the physics when the total excitation number is varied.

VII. SWEEP-RATE DEPENDENCE AND PHOTON NUMBER DEPENDENCE

So far we have seen that the quantum signature of chaos is consistent with the semiclassical prediction for relatively larger values of N. Here we investigate the chaotic features when the total excitation N is varied. In Fig. 6(a) we plot the efficiency $P = \langle \hat{n}_c \rangle_{\text{end}}/N$, where $\langle \hat{n}_c \rangle_{\text{end}}$ is the expectation value of cavity-c population at the end of the STIRAP scheme. The reduction in efficiency with slower sweep rates describes the presence of chaos [16,54]. Such an outcome originates solely due to the fact that a slower sweep permits the system spending a longer time within the chaotic window and enhances the spreading of the evolving state (see Fig. 5). Note

that here the analysis is for the closed-system case. For an open-quantum system scenario, dissipation also contributes to reducing efficiency for slower sweep rates (see Sec. IX). For interesting studies on open-system adiabatic evolution and the open STIRAP problem see Refs. [70,71]. Another aspect of Fig. 6(a) is the appearance of chaotic features with the varying photon number N. In Fig. 6(a) P is plotted for various N by keeping the characteristic parameters $J_{1,2}N$, ΔN, and $g_c\sqrt{N}$ fixed [14]. We observe that up to some N (e.g., $N = 8$ for $1/\tau = 0.003K$) the efficiency smoothly increases for a particular $1/\tau$. This is due to the fact that with increasing N P becomes larger compared to the excitation shared with the qubit in cavity c. The cavity-c state entangles photon and qubit degrees of freedom. Following this there is a sudden decrease in efficiency with further increment of N and a nonmonotonic jagged behavior thereafter. P in this regime of N considerably varies for various $1/\tau$ values and decreases with smaller $1/\tau$. Therefore, emergence of chaos demands a certain level of complexity in the quantum system and the complexity results from larger photon number. To clarify this point we plot Figs. 6(b) and 6(c), where the *widely*-avoided-crossing feature [as pointed out in Sec. III and marked by circle in Fig. 6(c)] can only be seen in Fig. 6(c) for $N = 10$. This feature in the eigenspectrum nicely correlates with the onset of chaotic (jagged) behavior in Fig. 6(a). Furthermore, OTOC plots in Figs. 6(d)–6(f) confirm chaotic eigenstates in the encircled region of Fig. 6(c). Another interesting observation is that the efficiency for faster sweep rates monotonically increases for larger N, whereas for slower rates its behavior is jagged. This hints that chaotic disruption takes place at slower sweep rates, whereas a sufficiently faster sweep dodges such effects. In other words, during the slow dynamics (with slower sweep rates) the system spends a longer time within the chaotic window producing more damage to the adiabatic passage. This feature is contrastingly different from that of a standard STIRAP (with $g_{a,b,c} = 0$), where the adiabatic passage performs better with slower sweep rates.

VIII. LEVEL SPACING STATISTICS

This section deals with level spacing statistics for the Hamiltonian given by Eq. (1). The chaoticity measure can be extracted from the distribution of the correlation parameter r_n of adjacent energy levels. r_n is given by

$$r_n = \frac{\min\{s_\nu, s_{\nu-1}\}}{\max\{s_\nu, s_{\nu-1}\}}, \tag{15}$$

where $s_\nu = E_{\nu+1} - E_\nu$ measures the spacing of nearest-neighbor energy levels with ordered E_ν. An average of r_n over a small energy window is denoted by $\langle r\rangle$ and serves as a good measure for chaoticity. Regular behavior with uncorrelated energy levels is characterized by $\langle r\rangle \approx 0.386$ for Poisson distribution, whereas a chaotic phase with strong level repulsion is characterized by $\langle r\rangle \approx 0.536$ for Gaussian orthogonal ensemble (GOE) distribution [72–74]. Any intermediate value for $\langle r\rangle$ reflects a mixed phase space having both chaotic and quasi-integrable regions. Such measure is advantageous compared to the traditional level statistics because it is independent of local density of levels.

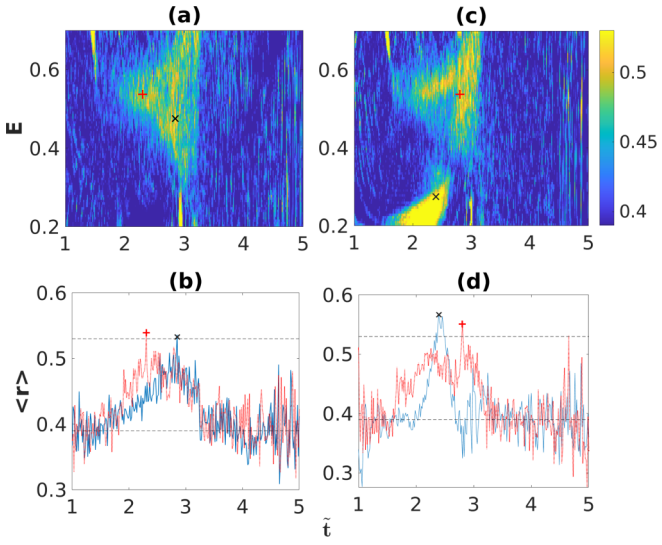

FIG. 7. Level spacing statistics with $N = 80$ and $\Delta = 0.125K$ for (a) $g_c = K$ and (c) $g_c = 1.5K$. The color coding is displayed according to $\langle r\rangle$ values. Panels (b) and (d) plot $\langle r\rangle$ for fixed energy levels corresponding to panels (a) and (c), respectively. Peak values for dotted red and solid blue plots are marked by "+" and "×," respectively. Symbols in panels (b) and (d) correspond to similar symbols in panels (a) and (c), respectively. Horizontal dashed lines in panels (b) and (d) mark the values 0.536 and 0.386, respectively.

In Fig. 7 we present level spacing statistics as explained above and observe chaotic stages during the course of STIRAP. Comparing Figs. 7(b) and 7(d) we see enhancement of chaoticity with increasing g_c value. Here we choose very strong g_c as we do not get strong enough level repulsion for smaller values of g_c. Moreover, large N is used to attain a dense spectrum and relatively accurate statistics. Here we should mention that the OTOC measure is more reliable and definitive (compared to level statistics) when chaoticity of specific energy levels is of interest [48].

IX. OPEN-SYSTEM DYNAMICS

The analysis so far deals with a closed system. However, a realistic cavity-QED system is affected by various decay channels and requires an open-quantum system treatment. In this section we treat the problem with Lindblad formalism and numerically solve the Lindblad master equation given by

$$\dot{\hat{\rho}}(t) = -i[\hat{H}, \hat{\rho}(t)] + \kappa\{\mathcal{L}[\hat{a}] + \mathcal{L}[\hat{b}] + \mathcal{L}[\hat{c}]\} + \gamma\mathcal{L}[\hat{s}_c^-], \tag{16}$$

where $\mathcal{L}[\hat{A}] = [2\hat{A}\hat{\rho}(t)\hat{A}^\dagger - \hat{A}^\dagger\hat{A}\hat{\rho}(t) - \hat{\rho}(t)\hat{A}^\dagger\hat{A}]/2$. κ and γ are decay rates for cavity photons and qubit, respectively. In Fig. 8 we plot the dissipative dynamics of cavity-QED STIRAP for two sweep rates. Comparing Figs. 8(a) and 8(b) we observe decrease of transfer efficiency with slower dynamics for fixed decay rates. This feature is as expected and demands a sweep rate $1/\tau \gg \kappa, \gamma$ to achieve considerable efficiency. Comparing Figs. 5(a) and 8(a) we see that our closed-system analysis holds well as long as $1/\tau \gg \kappa, \gamma$. In fact, both in Figs. 5(a) and 8(a) cavity b starts getting populated within the chaotic window.

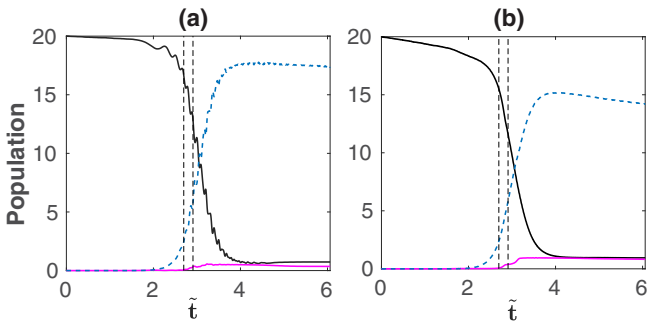

FIG. 8. Lindblad dynamics of n_a (solid black), n_b [solid magenta (gray)], and n_c (dashed blue) for (a) $1/\tau = 0.0121K$ and (b) $1/\tau = 0.003K$. Dissipation rates are given by $\kappa = \gamma = 10^{-4}K$.

As an important future direction it would be interesting to analyze the spectrum statistics of the full Liouvillian of the problem and characterize chaos for an open STIRAP problem [75,76]. As we have already noticed that the closed nonlinear STIRAP has a rich structure of mixed phase space, its dissipative version becomes more complex. This requires extensive analysis of the Liouvillian spectrum and will be dealt elsewhere.

X. CONCLUSION AND DISCUSSION

In this paper we have investigated the quantum signatures of chaos in a c-QED-based STIRAP. Throughout the paper we deal mostly with a Hermitian case but in a realistic system non-Hermitian contributions are activated through cavity loss and qubit decay. However, our analysis can well be justified when the decay rates are considerably smaller than the sweep rate (see supplementary material of [16]). In this situation the STIRAP scheme is completed well before the dissipation affects it significantly.

Our analysis is demonstrated in an experimentally realizable setup of c-QED STIRAP. Well-developed techniques of high-precision state preparation, measurement, and control of the cavity-QED system make c-QED STIRAP an interesting platform for testing quantum chaos signatures and design protocols for efficient population transfer in nonlinear realistic systems. Experimental determination of OTOC is a challenging task because it requires time-reversal evolution in principle [43,46]. This would require engineering the Hamiltonian to reverse its sign. The realizability of OTOC measurement in cavity-QED systems has been explored for large spin systems [77] and atomic ensembles [33]. The possible engineering of photon-qubit interaction includes phase manipulation in dispersive Jaynes-Cummings interaction [78] and phase-shifting gate operation on the qubit [79]. Furthermore, the intercavity photon tunneling can be tuned via tunable couplers [80,81]. However, a detailed analysis is needed to develop a concrete strategy to overcome such hurdle [43] in the studied case. As a future direction, it is interesting to extend such protocols in larger c-QED networks and investigate steady-state properties in a driven-dissipative version of the studied case.

[1] J. I. Cirac, P. Zoller, H. J. Kimble, and H. Mabuchi, Phys. Rev. Lett. **78**, 3221 (1997).
[2] J. Long, H. S. Ku, X. Wu, X. Gu, R. E. Lake, M. Bal, Y. X. Liu, and D. P. Pappas, Phys. Rev. Lett. **120**, 083602 (2018).
[3] B. Vogell, B. Vermersch, T. E. Northup, B. P. Lanyon, and C. A. Muschik, Quantum Sci. Technol. **2**, 045003 (2017).
[4] S. Kato, N. Német, K. Senga, S. Mizukami, X. Huang, S. Parkins, and T. Aoki, Nat. Commun. **10**, 1160 (2019).
[5] N. Meher, S. Sivakumar, and P. K. Panigrahi, Sci. Rep. **7**, 9251 (2017).
[6] A. Biswas and G. S. Agarwal, Phys. Rev. A **70**, 022323 (2004).
[7] Q. A. Turchette, C. J. Hood, W. Lange, H. Mabuchi, and H. J. Kimble, Phys. Rev. Lett. **75**, 4710 (1995).
[8] A. Rauschenbeutel, G. Nogues, S. Osnaghi, P. Bertet, M. Brune, J. M. Raimond, and S. Haroche, Phys. Rev. Lett. **83**, 5166 (1999).
[9] M. S. Zubairy, M. Kim, and M. O. Scully, Phys. Rev. A **68**, 033820 (2003).
[10] M. J. Hartmann, F. G. S. Brandão, and M. B. Plenio, Nat. Phys. **2**, 849 (2006).
[11] J. J. Mendoza-Arenas, S. R. Clark, S. Felicetti, G. Romero, E. Solano, D. G. Angelakis, and D. Jaksch, Phys. Rev. A **93**, 023821 (2016).
[12] R. Coto, M. Orszag, and V. Eremeev, Phys. Rev. A **91**, 043841 (2015).
[13] J. Jin, D. Rossini, M. Leib, M. J. Hartmann, and R. Fazio, Phys. Rev. A **90**, 023827 (2014).
[14] S. Schmidt, D. Gerace, A. A. Houck, G. Blatter, and H. E. Türeci, Phys. Rev B **82**, 100507(R) (2010).
[15] A. Dey and M. Kulkarni, Phys. Rev. A **101**, 043801 (2020).
[16] A. Dey and M. Kulkarni, Phys. Rev. Research **2**, 042004(R) (2020).
[17] M. Boissonneault, J. M. Gambetta, and A. Blais, Phys. Rev. A **79**, 013819 (2009).
[18] J. Raftery, D. Sadri, S. Schmidt, H. E. Türeci, and A. A. Houck, Phys. Rev. X **4**, 031043 (2014).
[19] S. Hughes and C. Roy, Phys. Rev. B **85**, 035315 (2012).
[20] Y. Lahini, F. Pozzi, M. Sorel, R. Morandotti, D. N. Christodoulides, and Y. Silberberg, Phys. Rev. Lett. **101**, 193901 (2008).
[21] J. Larson and D. H. J. O'Dell, J. Phys. B **46**, 224015 (2013).
[22] M. A. B. Magnani, B. L. del-Carpio, J. C. Carlos, S. L. Hernández, and J. G. Hirsch, Phys. Scr. **92**, 054003 (2017).
[23] J. Chávez-Carlos, B. López-del-Carpio, M. A. Bastarrachea-Magnani, P. Stránsky, S. Lerma-Hernández, and L. F. Santos, and J. G. Hirsch, Phys. Rev. Lett. **122**, 024101 (2019).
[24] C. Gogolin and J. Eisert, Rep. Prog. Phys. **79**, 056011 (2016).
[25] G. B. Lemos and F. Toscano, Phys. Rev. E **84**, 016220 (2011).
[26] W. H. Zurek, Phys. Scr. T **76**, 186 (1998).
[27] L. Chotorlishvili and A. Ugulava, Physica D **239**, 103 (2010).
[28] G. B. Lemos, R. M. Gomes, S. P. Walborn, P. H. Souto Ribeiro, and F. Toscano, Nat. Commun. **3**, 1211 (2012).

[29] H. Ammann, R. Gray, I. Shvarchuck, and N. Christensen, Phys. Rev. Lett. **80**, 4111 (1998).

[30] F. L. Moore, J. C. Robinson, C. Bharucha, P. E. Williams, and M. G. Raizen, Phys. Rev. Lett. **73**, 2974 (1994).

[31] A. Frisch, M. Mark, K. Aikawa, F. Ferlaino, J. L. Bohn, C. Makrides, A. Petrov, and S. Kotochigova, Nature (London) **507**, 475 (2014).

[32] C. Hainaut, P. Fang, A. Rançon, J.-F. Clément, P. Szriftgiser, J.-C. Garreau, C. Tian, and R. Chicireanu, Phys. Rev. Lett. **121**, 134101 (2018).

[33] B. Swingle, G. Bentsen, M. Schleier-Smith, and P. Hayden, Phys. Rev. A **94**, 040302(R) (2016).

[34] G. Zhu, M. Hafezi, and T. Grover, Phys. Rev. A **94**, 062329 (2016).

[35] E. P. Wigner, Proc. Cambridge Philos. Soc. **47**, 790 (1951).

[36] F. M. Izrailev, Phys. Rep. **196**, 299 (1990).

[37] A. Dey, D. Cohen, and A. Vardi, Phys. Rev. A **99**, 033623 (2019).

[38] A. I. Larkin and Y. N. Ovchinnikov, Zh. Eksp. Teor. Fiz. **55**, 226 (1969) [JETP **28**, 1200 (1969)].

[39] K. Hashimoto, K. Murata, and R. Yoshii, J. High Energy Phys. 10 (2017)138.

[40] P. Hayden and J. Preskill, J. High Energy Phys. 09 (2007) 120.

[41] S. H. Shenker and D. Stanford, J. High Energy Phys. 03 (2014) 067.

[42] J. Maldacena, S. H. Shenker, and D. Stanford, J. High Energy Phys. 08 (2016) 106.

[43] É. Lantagne-Hurtubise, S. Plugge, O. Can, and M. Franz, Phys. Rev. Res. **2**, 013254 (2020).

[44] B. Swingle, Nat. Phys. **14**, 188 (2018).

[45] J. Li, R. Fan, H. Wang, B. Ye, B. Zeng, H. Zhai, X. Peng, and J. Du, Phys. Rev. X **7**, 031011 (2017).

[46] M. Gärttner, J. G. Bohnet, A. Safavi-Naini, M. L. Wall, J. J. Bollinger, and A. M. Rey, Nat. Phys. **13**, 781 (2017).

[47] K. A. Landsman, C. Figgatt, T. Schuster, N. M. Linke, B. Yoshida, N. Y. Yao, and C. Monroe, Nature (London) **567**, 61 (2019).

[48] T. Akutagawa, K. Hashimoto, T. Sasaki, and R. Watanabe, J. High Energy Phys. 08 (2020) 013.

[49] N. V. Vitanov, A. A. Rangelov, B. W. Shore, and K. Bergmann, Rev. Mod. Phys. **89**, 015006 (2017).

[50] K. Bergmann, H. Theuer, and B. W. Shore, Rev. Mod. Phys. **70**, 1003 (1998).

[51] E. M. Graefe, H. J. Korsch, and D. Witthaut, Phys. Rev. A **73**, 013617 (2006).

[52] B. Wu and Q. Niu, Phys. Rev. A **61**, 023402 (2000).

[53] Y.-A. Chen, S. D. Huber, S. Trotzky, I. Bloch, and E. Altman, Nat. Phys. **7**, 61 (2011).

[54] A. Dey, D. Cohen, and A. Vardi, Phys. Rev. Lett. **121**, 250405 (2018).

[55] A. Dey and A. Vardi, Phys. Rev. A **101**, 053627 (2020).

[56] A. S. Parkins, P. Marte, P. Zoller, and H. J. Kimble, Phys. Rev. Lett. **71**, 3095 (1993).

[57] L. B. Chen, M. Y. Ye, G. W. Lin, Q.-H. Du, and X.-M. Lin, Phys. Rev. A **76**, 062304 (2007).

[58] L. D. Landau, Phys. Z. Sowjetunion **2**, 46 (1932).

[59] C. Zener, Proc. R. Soc. A **137**, 696 (1932).

[60] E. C. G. Stuckelberg, Helv. Phys. Acta **5**, 369 (1932).

[61] E. Majorana, Nuovo Cimento **9**, 45 (1932).

[62] M. Casartelli, E. Diana, L. Galgani, and A. Scotti, Phys. Rev. A **13**, 1921 (1976).

[63] G. Benettin, L. Galgani, A. Giorgilli, and J.-M. Strelcyn, Meccanica **15**, 9 (1980).

[64] G. Benettin, L. Galgani, A. Giorgilli, and J.-M. Strelcyn, Meccanica **15**, 21 (1980).

[65] G. Benettin, L. Galgani, and J.-M. Strelcyn, Phys. Rev. A **14**, 2338 (1976).

[66] T. A. Elsayed, B. Hess, and B. V. Fine, Phys Rev E **90**, 022910 (2014).

[67] A. S. Bamzai and B. M. Deb, Rev. Mod. Phys. **53**, 95 (1981).

[68] A. Redondo and J. C. Marshall, J. Chem. Phys. **91**, 5492 (1989).

[69] D. Dast, D. Haag, H. Cartarius, and G. Wunner, Phys. Rev. A **93**, 033617 (2016).

[70] M. S. Sarandy and D. A. Lidar, Phys. Rev. A **71**, 012331 (2005).

[71] T. Mathisen and J. Larson, Entropy **20**, 20 (2018).

[72] V. Oganesyan and D. A. Huse, Phys. Rev. B **75**, 155111 (2007).

[73] N. D. Chavda, H. N. Deota, and V. K. B. Kota, Phys. Lett. A **378**, 3012 (2014).

[74] Y. Y. Atas, E. Bogomolny, O. Giraud, and G. Roux, Phys. Rev. Lett. **110**, 084101 (2013).

[75] L. Sá, P. Ribeiro, and T. Prosen, Phys. Rev. X **10**, 021019 (2020).

[76] G. Akemann, M. Kieburg, A. Mielke, and T. Prosen, Phys. Rev. Lett. **123**, 254101 (2019).

[77] J. Marino and A. M. Rey, Phys. Rev. A **99**, 051803(R) (2019).

[78] D. Lv, S. An, M. Um, J. Zhang, J.-N. Zhang, M. S. Kim, and K. Kim, Phys. Rev. A **95**, 043813 (2017).

[79] M. Ezawa, Phys. Rev. Res. **2**, 023278 (2020).

[80] B. Peropadre, D. Zueco, F. Wulschner, F. Deppe, A. Marx, R. Gross, and J. J. Garcia-Ripoll, Phys. Rev. B **87**, 134504 (2013).

[81] S. Schmidt and J. Koch, Ann. Phys. (Berlin) **525**, 395 (2013).